

Investigation of the Eightwise Switching Mechanism and Its Suppression in SrTiO₃ Modulated by Humidity and Interchanged Top and Bottom Platinum and LaNiO₃ Electrode Contacts

Eva Sediva, William J. Bowman, Juan Carlos Gonzalez-Rosillo, and Jennifer L. M. Rupp*

Memristive devices are hardware components for applications in neuromorphic computing, memories, and logic computation. This work contributes to the ongoing debate on the switching mechanism of eightwise polarity in SrTiO₃-based resistive switches. Specifically the effect of atmospheric humidity on the materials defect chemistry and switching properties is considered. Asymmetric devices are designed by exchanging the top and bottom positions of Pt and LaNiO₃ electrodes allowing for a separate analysis of the top and the bottom metal-oxide interfaces. Under dry atmospheres the switching hysteresis is enhanced with a top Pt contact and suppressed with a bottom Pt contact. It is argued that the buried position and dense microstructure of the bottom platinum impedes an oxygen vacancy driven switching mechanism. Under humid atmospheres eightwise switching occurs in both devices suggesting the presence of two switching mechanisms within the same eightwise switching polarity, namely, oxygen vacancy and hydroxide ion enabled switching. The findings help develop strategies to suppress eightwise switching by burying the active metal-oxide interface and ensuring dense electrode microstructures. Suppression of switching mechanisms relying on exchange with the environment is desirable for technological implementation of resistive switches and for strategies in stacking of memristive devices for memory and for neuromorphic hardware.

neuromorphic computing.^[5,6] The attractive properties enabling this variety of applications are the tunable time scales of their switching speeds down to sub-nanoseconds^[7] and nonvolatility up to 10 years^[8,9] combined with scalability down to a couple of nanometers and low power dissipation.^[10] Changes of resistance states in the oxides are facilitated by ion transport under high local electrical fields. The investigation of the influence of small scale effects such as space charges at metal-oxide interfaces and filaments on ionic transport are important for developing this technology.^[11] In general oxide-based memristive devices work on the principle of nonvolatile resistance change upon the application of an electrical potential.^[12] The switching mechanism is generally considered to be facilitated by internal redistribution of oxygen vacancies (defects) coupled to a valence change in the metal ion.^[1] Recently however, it has been shown that also the change in the relative humidity in the surrounding

1. Introduction

Oxide-based memristive devices have shown promise for future applications such as computer memory,^[1,2] logic^[3,4] and

atmosphere will change the resistive switching behavior of TaO_x,^[13,14] HfO_x,^[13] SrTiO₃,^[15,16] and TiO₂.^[17] Specifically, a primary study with Pt/SrTiO₃/Pt switching bits by Messerschmitt et al. investigated the influence of relative humidity on the current-voltage (*I*-*V*) properties, showing that switching can be suppressed or enabled depending on the humidity level.^[15] Heisig et al. confirmed with H₂¹⁸O isotope labeling experiments that oxygen from water incorporates into and oxidizes the SrTiO₃ switching oxide, and Tappertzhofen et al. showed that the catalytic activity toward water splitting of the electrode determines the ion incorporation extent and reaction rate.^[18] Of particular interest in relation to the humidity influence is the so-called “eightwise switching polarity mechanism,” schematically depicted in **Figure 1a**, since it has recently been confirmed by Cooper et al. that it relies on exchange of oxygen ions in the atmosphere.^[19] Using in situ transmission electron microscopy (TEM) they demonstrated that oxygen evolution and reincorporation in the top Pt electrode is responsible for the eightwise polarity switching mechanism in SrTiO₃. What remains unclear is specifically the role of the top electrode material choice and catalytic activity when exposed to the atmosphere. To probe this

E. Sediva, Dr. W. J. Bowman, Prof. J. L. M. Rupp
Electrochemical Materials
Department of Materials
ETHZ
Hönggerberggring 64, 8093 Zurich, Switzerland
E-mail: jrupp@mit.edu

E. Sediva, Dr. J. C. Gonzalez-Rosillo, Prof. J. L. M. Rupp
Electrochemical Materials
Department of Materials Science and Engineering
Massachusetts Institute of Technology
77 Massachusetts Av., Cambridge, MA 02139, USA

Prof. J. L. M. Rupp
Electrochemical Materials
Department of Electrical Engineering and Computer Science
Massachusetts Institute of Technology
77 Massachusetts Av., Cambridge, MA 02139, USA

DOI: 10.1002/aelm.201800566

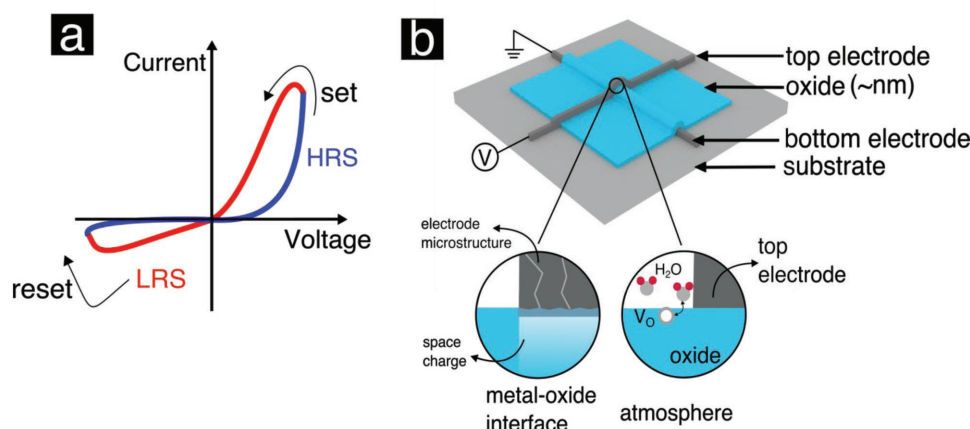


Figure 1. a) A schematic I - V curve with the eightwise resistive switching polarity. b) Schematic depiction of a thin film resistive switch grown on a substrate emphasizing the influence of the environmental humidity and metal-oxide interfacial properties.

we select SrTiO₃ as the switching material as it was recently benchmarked for the investigation of the eightwise polarity mechanism and will focus on an alternated top electrode versus its bottom electrode choice.^[19]

SrTiO₃ is a widely investigated material for resistive switching because it is on the one hand a technically well established oxide in high-voltage capacitors and on the other hand has a well known defect chemistry.^[20,21] Resistive switching devices were demonstrated on donor (i.e., Nb) doped,^[22–24] acceptor (i.e., Fe) doped^[25,26] and nominally undoped SrTiO₃.^[19,27–29] Nb is a shallow donor dopant that creates a strong n-type conductivity with a very low concentration of oxygen vacancies^[30] while Fe forms an acceptor level in the SrTiO₃ band gap.^[31] In Fe doped SrTiO₃ oxygen vacancies were suggested to be responsible for the resistive switching^[25] while in Nb doped SrTiO₃ it was both reoxidation through the top Pt electrode^[23] and electronic charge trapping at the metal-oxide interface.^[22] The switching polarity has been consistently different with both dopants, Nb exhibiting eightwise polarity^[22,23] and Fe counter-eightwise or both competing polarities.^[25,29,32,33] Competing switching polarities dependent on the electrical field are possible in a single switching bit^[25,29] and a debate in the literature has been ongoing about the switching mechanism in devices with the eightwise polarity.^[19,34] Recently, Cooper et al. proposed oxygen evolution and reincorporation into the high work function platinum electrode as the mechanism in undoped SrTiO₃.^[19] However, a study acknowledging the materials defect chemistry upon varying the humidity and the top electrodes is still missing.

Resistive switching is controlled on the interfaces defined by the choice of materials for electrode-switching oxide pair. Electrodes are rationally chosen to stabilize the switching behavior usually with a bottom ohmic contact and a high work function Schottky top contact resulting often in highly rectifying I - V curves with a strong asymmetry in the switching response, Figure 1a. It is then generally assumed that the switching event happens at the interface with the high work function metal contact that forms the Schottky barrier by altering the barrier properties.^[35] However, other aspects of the interface such as the interface state

density can affect the switching location. For example, it was shown in Nb:SrTiO₃ that changes in the growth condition of the platinum electrode control the occurrence and magnitude of the switching hysteresis.^[22,24] The resistive switching hysteresis was suppressed with epitaxial Pt contacts sputtered at high temperatures and enhanced with e-beam evaporated Pt contacts at room temperature. Charge trapping in an insulating defective interfacial layer was proposed to be the switching mechanism. Such interfacial layers were suggested to originate from unintentional highly energetic metal deposition inducing defects in the oxide material^[22,36] or also from cation nonstoichiometry at the oxide surface.^[30] Such changes in interfacial properties can happen, for example, in a classic two-terminal device in cross-plane geometry where the first metal electrode is grown on a substrate whereas the subsequently processed top electrode is grown on the switching oxide. Importantly, this can lead to changes in nucleation and growth of the oxide and electrodes, its defect density, chemistry, or grain characteristics resulting in different top and bottom electrode interface properties.

Second, the control of the materials bulk and interfacial defect chemistry can come from the atmospheric humidity by material exchange from the top electrode-oxide interface, Figure 1b. Using H₂¹⁸O exchange experiments on SrTiO₃ Heisig et al. recently confirmed that oxygen incorporation from humidity happens at room temperature with the driving force of high electric fields rather than Joule heating in the switching oxide.^[16] The incorporation through filling of oxygen vacancies can be defined using Kröger-Vink notation^[13]



Protons can be also directly incorporated into oxides, where charge compensation of two electrons becomes necessary for charge neutrality. The corresponding equation is^[13]



In this case the hydroxide ions are compensated by electrons and hydrogen acts as a donor dopant. Generally, although

proton-based resistive switching has been demonstrated to work,^[37,38] this is still a young field and far from being understood.

The defect chemical changes that humidity induces can affect the Schottky contact barrier and space charge region ultimately changing the switching behavior. The extent and the rate of humidity incorporation are strongly influenced by the electrode electrocatalytic activity toward the water redox reaction, which was systematically studied for SiO₂-based reference switching devices with Cu and Ag active electrodes by Tappertzhofen et al.^[18] In summary, investigations of eightwise polarity resistive switching have been often limited to studies of the top metal-oxide Schottky contact concentrating separately on electronic interfacial transport properties^[22,39] or humidity uptake.^[15,16] However studies of the effect of varying the electrocatalytic activity of the top electrode exposed to the humid atmosphere on the valence change oxygen anion based switching devices are still missing.

Through this study we investigate the humidity influence on the eightwise polarity switching mechanism by separately considering the top and bottom metal-oxide interface contributions. For this, we process two memristive device architectures in which we alternate the stacking sequence of the bottom and the top electrodes, being Pt or LaNiO₃ electrode films, while keeping the undoped SrTiO₃ switching oxide in between. The change in electrode deposition sequence allows investigation of the resistive switching response in two aspects.

First, we change the material of the electrode exposed to atmosphere (top) with respect to the buried electrode (bottom) using Pt and LaNiO₃. This allows in the study to separate the impact of humidity level changes on the Pt and LaNiO₃ interfaces with SrTiO₃. Second, Pt serves as the electrode with the higher work function that enables us to intentionally engineer an asymmetry of the Schottky barriers into our model devices. Thereby we can test the impact of humidity level changes on the open or buried high Schottky barrier Pt–SrTiO₃ interface, previously accessible only in symmetrical cells^[27] or as the top metal contact.^[16,19] We identify two switching mechanisms within the same eightwise polarity depending on the atmospheric humidity levels, which we interpret by changes in the materials defect chemistry. Ultimately we demonstrate that we can suppress eightwise resistive switching in dry atmospheres with a buried and dense Pt electrode. This has technological relevance since the suppression of mechanisms relying on material exchange with the atmosphere is desirable since control of the surrounding atmosphere during device operation would be difficult. Eightwise switching can also be in competition with its coexistent counter polarity mechanism^[25,29] degrading device response. Our findings offer strategies on how to suppress eightwise resistive switching by burying the high Schottky barrier contact and ensuring dense electrode microstructure.

2. Results and Discussion

2.1. Fabrication of SrTiO₃-Based Memristive Devices with Alternate Electrode Sequences and Materials

We fabricate resistive switching devices with alternating top and bottom electrode arrangements namely LaNiO₃(bottom)/

SrTiO₃/Pt(top) and Pt(bottom)/SrTiO₃/LaNiO₃(top) deposited on MgO substrates. We present schematics of the two device architectures and their corresponding microstructures imaged using scanning TEM (STEM) annular dark field and TEM bright field in a cross-sectional view in Figure 2a–c for the LaNiO₃(bottom)/SrTiO₃/Pt(top) and in Figure 2d–f for Pt(bottom)/SrTiO₃/LaNiO₃(top) device.

Low-magnification cross-section TEM images, Figure 2c,f, confirm the growth of dense thin films in all the constituent layers. Independent of the electrode growth sequence, we can confirm polycrystalline columnar grain structure with comparable average grain sizes of 17 to 19 ± 3 nm for the SrTiO₃ switching oxide based on analysis of the bright field TEM images in Figure 2c,f. The microstructures and the grain sizes of the switching oxide are very similar between the two model devices, which is important for the comparison of their electrical response. Now we turn to the high resolution TEM study of the interfaces between the Pt electrode and the SrTiO₃ switching oxide. In the LaNiO₃(bottom)/SrTiO₃/Pt(top) device, Figure 2g, the metal electrode is exposed to air, and in the Pt(bottom)/SrTiO₃/LaNiO₃(top) device, Figure 2h, the Pt electrode is buried between the substrate and the switching oxide. First, in the case where Pt is the top, the electrode room temperature electron beam evaporation yields a nanocrystalline film, Figure 2g. When the Pt electrode is on top, the interface morphology between Pt and SrTiO₃ is the result of the SrTiO₃ thin film columnar growth, which produces a faceted top surface with a roughness of about 10 nm and an enhanced concentration of higher index steps and corner lattice sites. Second, when the Pt electrode is buried underneath the SrTiO₃, Figure 2h, the interface exhibits a roughness of about 1 nm, and is comprised of an abrupt contact between low-index surface terminations in the oxide and metal. Also, the rather coherent interface is of considerably higher crystalline quality than that of the Pt top contact. The microstructure differences between the bottom and the top platinum films are further depicted in Figure S2 of the Supporting Information with scanning TEM high-angle annular dark field images. The LaNiO₃ electrode contact deposited at elevated temperatures (500 °C) in both devices produces a dense thin film. Similar to the Pt the top LaNiO₃–SrTiO₃ interface contact is faceted with a roughness of about 10 nm while the bottom produces a smooth abrupt contact.

We conclude based on the TEM analysis of the nanostructures for the resistive switching devices, that the electrode–electrolyte material deposition sequence does considerably affect the interface morphology. Between the top and bottom electrode–SrTiO₃ contact we observe an interface roughness difference of 9 nm and in the case of Pt electrode microstructure change from dense to nanocrystalline, which both can affect the defect density of interface states. This can be rationalized because the bottom electrode layer must be annealed at elevated temperatures prior to deposition of SrTiO₃, producing a smooth high crystalline quality substrate upon which SrTiO₃ grows. However the top Pt contact deposited at room temperature has noncrystalline morphology, as it was not annealed at higher temperatures. This difference between the top and the bottom interfaces is crucial to understand the switching behavior of the films. The SrTiO₃ switching oxide grain size and morphology remain unaffected, as its thermal treatment history is the same in both devices.

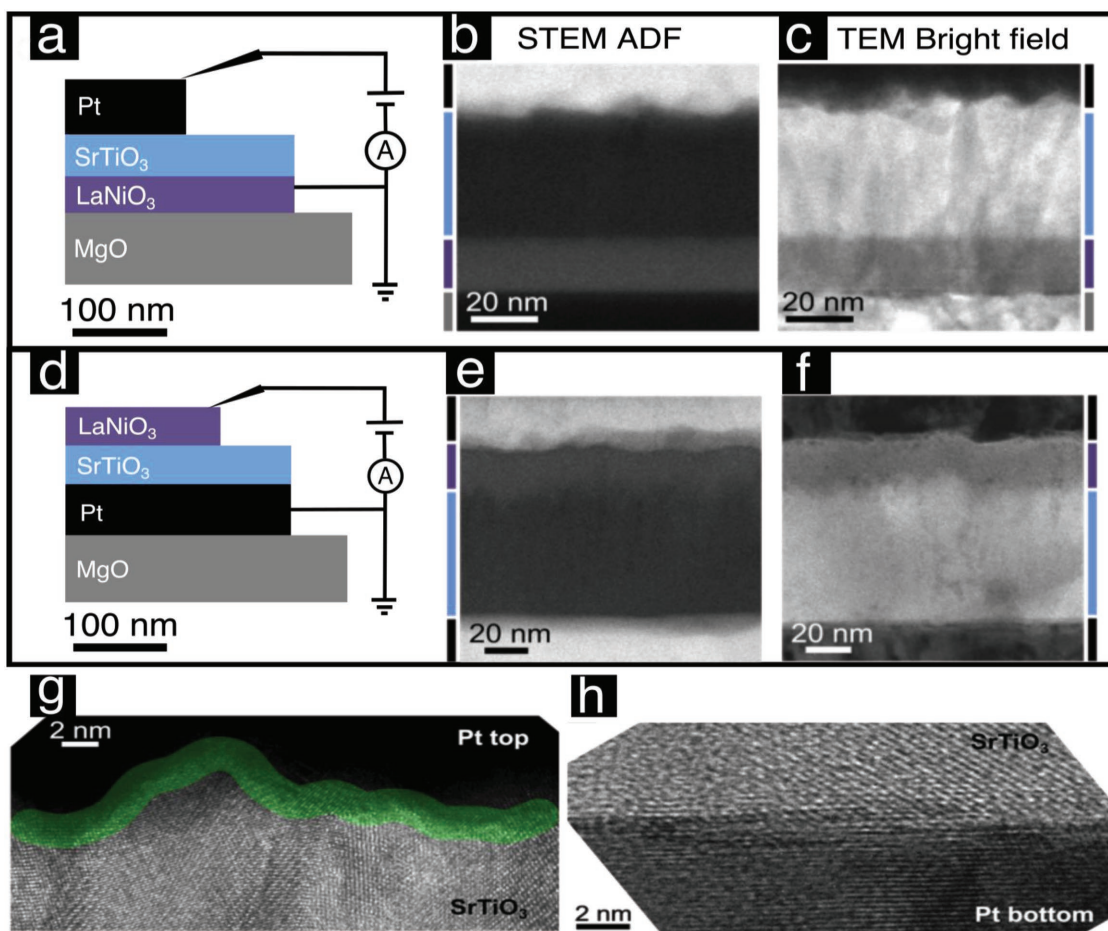


Figure 2. Transmission electron microscopy (TEM) device characterization. a–c) LaNiO_3 (bottom)/ SrTiO_3 /Pt(top) device. d–f) Pt(bottom)/ SrTiO_3 / LaNiO_3 (top) device. a, d) Schematic representations. Low-magnification b, e) scanning TEM (STEM) annular dark field (ADF) and c, f) bright field images. g, h) High-resolution TEM (HRTEM) images of the Pt– SrTiO_3 g) top contact and h) bottom contact interfaces. The Pt contact interface length used for contact area measurement is highlighted in (g).

The nanocrystalline Pt electrode morphology is consistent with previous results showing nanometer sized Pt grains with scanning tunneling microscopy proving also that oxygen permeation through the grain boundaries is possible.^[40] Electron beam evaporated platinum contacts on SrTiO_3 are known to produce surface damage upon deposition affecting I – V properties of the devices.^[22,36,41] This damage can be avoided by using Pt bottom contacts deposited on the substrate rather than the switching oxide thin film. In the following, we will now investigate the implications of changing the top electrode material, Pt versus LaNiO_3 , under varying humidity levels on the property of resistive switching by electrochemical testing.

2.2. Humidity Influence on Device's I – V Characteristics

To access the role of humidity on the resistive switching response with interchanged electrode positions we probe the resistive switching response by cyclic voltammetry measurements under controlled atmospheres of 40% and 5% relative humidity (RH) in synthetic air. No electroforming was used on either of the devices in agreement with eightwise switching for

symmetric Pt/ SrTiO_3 /Pt devices.^[27] In addition, the absence of electroforming impedes the formation of oxygen bubbles in the top electrode.^[42]

The resulting I – V curves for Pt and LaNiO_3 top electrodes and the according alternative bottom electrode material are depicted in comparison in **Figure 3a,b**.

First, we notice that independent of the top electrode material choice the current increases with increasing humidity by about an order of magnitude in the LaNiO_3 (bottom)/ SrTiO_3 /Pt(top) device and by several orders of magnitude in the Pt(bottom)/ SrTiO_3 / LaNiO_3 (top) device. This is consistent with previous reports on platinum contacts with TiO_2 ,^[17] $\text{Ba}_{1-x}\text{Sr}_x\text{TiO}_3$,^[43] Ta_2O_5 and HfO_2 ,^[13] 0.02 mol% Nb-doped SrTiO_3 ,^[44] and undoped SrTiO_3 ^[15] under high electric fields, which show increased leakage currents under hydrogen or water exposures. Second, under higher humidity levels of 40% RH both devices exhibit rectification behavior with larger currents when applying a positive bias with respect to the top electrode. Rectification is characteristic of a Schottky diode, which is governed by the metal contact with the higher work function being in our case Pt. This rectifying behavior is observed in the LaNiO_3 (bottom)/ SrTiO_3 /Pt(top) device, **Figure 3a**, however the

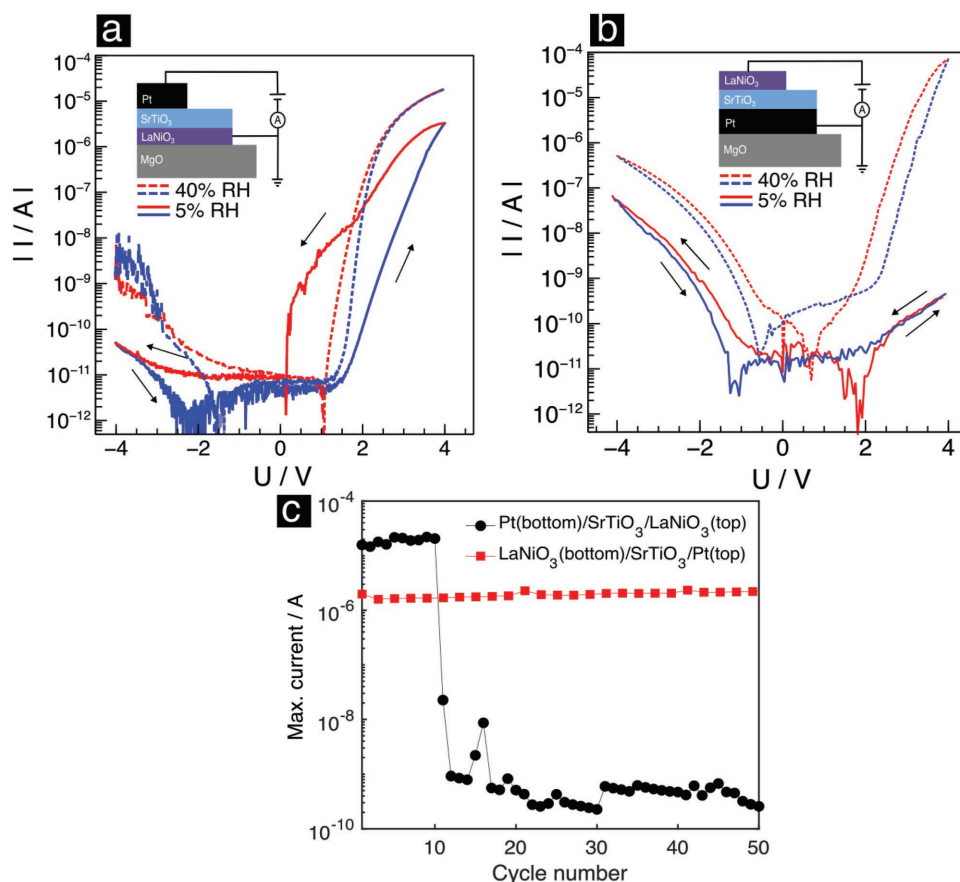


Figure 3. a, b) I - V curves of the two model devices under two different humidity levels of 5% and 40% RH. The high-resistance state is plotted in blue and the low resistance state in red. c) The evolution of the maximum current over 50 cycles when placing the device into a dry atmosphere of 5% RH.

opposite direction of rectification would be expected when Pt is the bottom contact in the Pt(bottom)/SrTiO₃/LaNiO₃(top) device, Figure 3b. This direction emerges only after lowering the humidity level to 5% RH where a current decrease at positive applied bias of about five orders of magnitude is observed. In Figure 3c we plot the maximum current evolution over 50 cycles for both devices after being placed under a 5%RH atmosphere. The response of the Pt(bottom)/SrTiO₃/LaNiO₃(top) device to the change in the relative humidity is not immediate and current decreases only after about 10 cycles at 50 mV s⁻¹, Figure 3c, and after about 20 cycles at 500 mV s⁻¹ (not shown). The time lag in the device response confirms the importance of the high electric field in the ion incorporation process. This is confirmed by recent studies showing that the electric field and sweep rate plays a key role in the oxygen incorporation.^[16,18] Also initial studies by Messerschmitt et al. show that the maximum current during the set process drops with humidity.^[15] The gradual response to the humidity change is in contrast to the LaNiO₃(bottom)/SrTiO₃/Pt(top) device, Figure 3c, where changes in the I - V hysteresis loop occur immediately. We argue that this difference between the two devices can be due to the difference between the top electrode materials exposed to the atmosphere. A faster device response can be expected from the device with a Pt top electrode given its higher catalytic activity toward water splitting. This agrees

with recent reports showing that the electrode catalytic activity influences the rate of reaction and the concentration of dissolved ions.^[18]

2.3. Humidity Influence on Device's Switching Response

First, we observe in both devices hysteretic behavior with the eightwise polarity meaning switching from high resistance (blue) to low resistance (red) state with a positive applied bias, Figure 3. The same switching polarity in both devices is an unexpected behavior considering that resistive switching polarity is defined by the sequence of the electrodes governed by the modulation of the Schottky barrier at the active interface (location of the switching event).^[45-47] The identical switching polarity in the two devices shows that the interface where the switching occurs must be at the same geometrical location in both devices. We argue that the same switching polarity is defined by the difference between the bottom and the top metal-oxide interface contacts as accessed by the high-resolution TEM (HRTEM) analysis, Figure 2g,h.

Second, in the LaNiO₃(bottom)/SrTiO₃/Pt(top) device the switching hysteresis opens under dry conditions, Figure 3a. An opening of the switching hysteresis implies a larger influence of mobile oxygen vacancies, whose higher density under dry

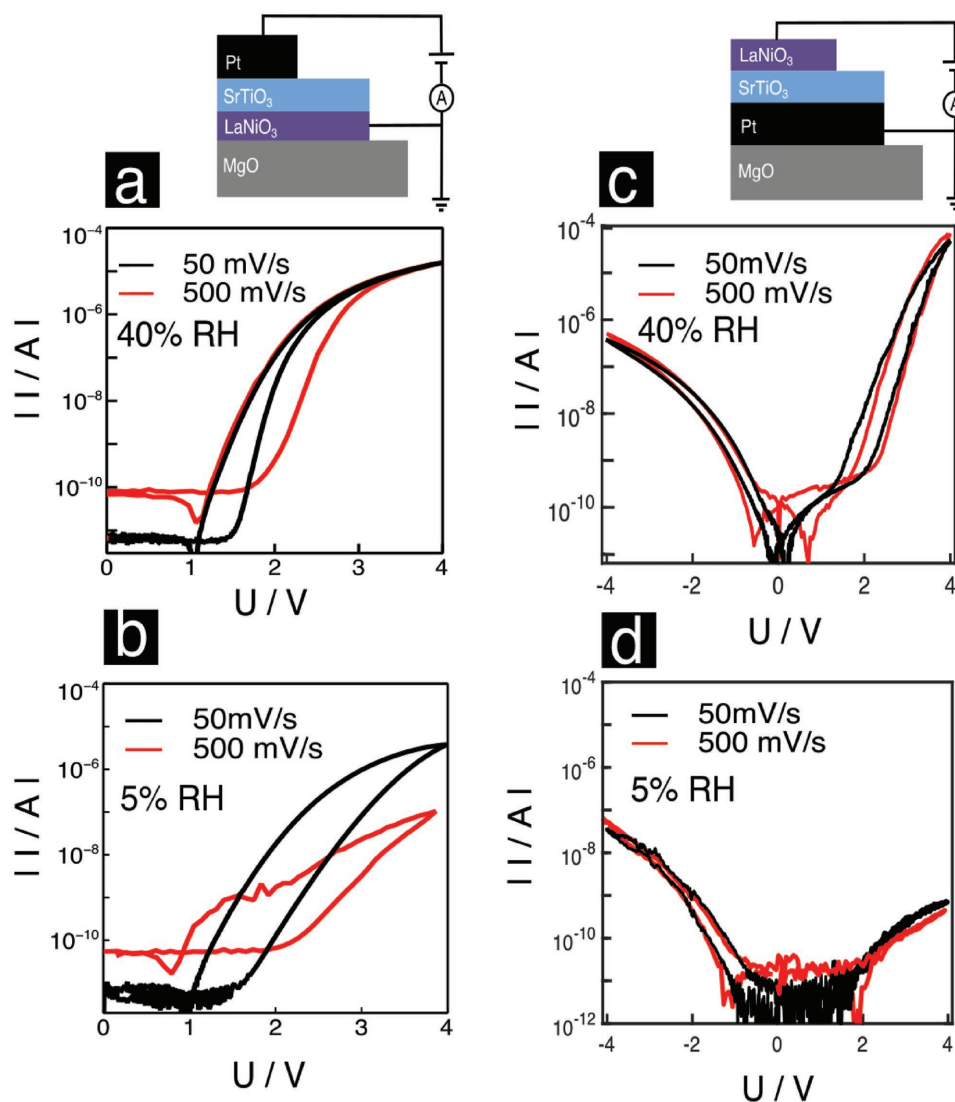


Figure 4. Influence of the sweeping speed on the I - V characteristics of the a,b) $\text{LaNiO}_3(\text{bottom})/\text{SrTiO}_3/\text{Pt}(\text{top})$ and c,d) $\text{Pt}(\text{bottom})/\text{SrTiO}_3/\text{LaNiO}_3(\text{top})$ device measured under a,c) 40% RH and b,d) 5% RH.

conditions (Equation (1)) can strengthen the (re)incorporation of oxygen into the Pt electrode^[19] aiding the switching process. This is in stark contrast to the $\text{Pt}(\text{bottom})/\text{SrTiO}_3/\text{LaNiO}_3(\text{top})$ device, Figure 3b, where a suppression of the switching hysteresis under dry conditions occurs meaning that neither the bottom Pt nor the top LaNiO_3 contact enable a switching mechanism aided by the oxygen vacancies in the same way as the top Pt contact does.

These results are supported by cyclic voltammetry measured under two different sweeping speeds of 50 and 500 mV s^{-1} , Figure 4. Here, the $\text{LaNiO}_3(\text{bottom})/\text{SrTiO}_3/\text{Pt}(\text{top})$ device, Figure 4a,b, exhibits a dependence of the maximum current on the sweep rate only under dry conditions. These kinetics are reminiscent of the ionic conductivity in the material causing redistribution of ionic charge carriers inside the thin film during the application of an electric field.^[27] By contrast, the $\text{Pt}(\text{bottom})/\text{SrTiO}_3/\text{LaNiO}_3(\text{top})$ device shows no sweep rate dependence of the current at either humidity level, Figure 4c,d,

which together with the suppression of the switching hysteresis under dry conditions suggest that neither the bottom Pt nor the top LaNiO_3 electrode supports an oxygen vacancy driven switching mechanism.

To probe the extent of the ion incorporation from humidity through the thickness of the thin film we measured the response of the $\text{LaNiO}_3(\text{bottom})/\text{SrTiO}_3/\text{Pt}(\text{top})$ device with a thicker SrTiO_3 switching oxide of 200 nm. According to sweep rate characteristics, Figure S3 of the Supporting Information, the ion incorporation did not occur to the same extent as the thinner (≈ 60 nm) concluding it is a bulk-limited diffusion process rather than surface.

In conclusion under humid conditions the switching event happens at the top electrode- SrTiO_3 contact, which can be caused by the relatively lower crystalline quality as compared to the bottom interface. The cause of this could be a combination of the surface damage caused by the top electrode deposition, higher SrTiO_3 surface roughness causing

an enhanced concentration of higher index steps and corner lattice sites or a different interface chemistry. The Pt(bottom)/SrTiO₃/LaNiO₃(top) device completely suppresses resistive switching under dry atmospheres, however enables under humid atmospheres when the SrTiO₃ thin film is oxidized and when protonic charge carriers are present. On the other hand, a top Pt contact enhances the switching hysteresis under dry conditions but does not completely suppress it in a humid atmosphere.

2.4. Parameters of the Pt–SrTiO₃ Interface in the LaNiO₃(Bottom)/SrTiO₃/Pt(Top) Device

2.4.1. Thermionic Emission

We discuss now the LaNiO₃(bottom)/SrTiO₃/Pt(top) device under moderate (40% RH) humidity levels with the thermionic emission model describing transport of electrons over the barrier.^[48] In the Pt(bottom)/SrTiO₃/LaNiO₃(top) device we do not expect transport over the Schottky barrier due to the opposite rectification direction than the position of the bottom Pt contact predicts. Therefore we do not directly apply the thermionic emission model on this device. We discuss further details in Figure S4 of the Supporting Information. We fit the *I*–*V* curve of the LaNiO₃(bottom)/SrTiO₃/Pt(top) device with the thermionic emission equation, Equation (3) (see also Figure 5a)

$$I(V) = AA^*T^2 \exp\left(-\frac{q\Phi_B}{k_B T}\right) \left(\exp\left(\frac{qV}{nk_B T}\right) - 1\right) \quad (3)$$

Here *A* is the contact surface area of the metal and the oxide, *A** is the Richardson constant, *q* is the elementary charge, Φ_B is the Schottky barrier height, *T* is the temperature, *k_B* is the Boltzmann constant, and *n* is the ideality factor which describes the deviation from the thermionic emission theory. The fitting parameters here were the ideality parameter *n* and the Schottky barrier height Φ_B giving the values of 3.67 and 2.32 for *n* and 1.43 and 1.07 eV for the barrier height for the low and high resistive states, respectively. The decrease in both values in the high resistance state is in accordance to literature results on resistive switching devices.^[22,39,49,50] The barrier heights are about 0.4 eV higher than from previous results using Nb:SrTiO₃,^[22,50] which can be due to the lower intrinsic doping levels when using nominally undoped SrTiO₃.

The fitted ideality parameters deviate from the ideal value of 1, which is not uncommon in metal-oxide contacts^[22,51] and based on previous literature reports^[22,52] we expect that an insulating interfacial layer exists at the relatively defective interface between the upper surface of the SrTiO₃ thin film and the Pt electrode. This would suggest that the applied voltage is partitioned between a interfacial layer and the adjacent charge carrier depletion width in the oxide.

Previously, the thermionic emission model has been reserved for the transport mechanism in donor doped Nb:SrTiO₃ with Pt,^[22,49] Au,^[52] SrRuO₃,^[39] and Ba_{1-x}K_xBiO₃^[53,54] contacts

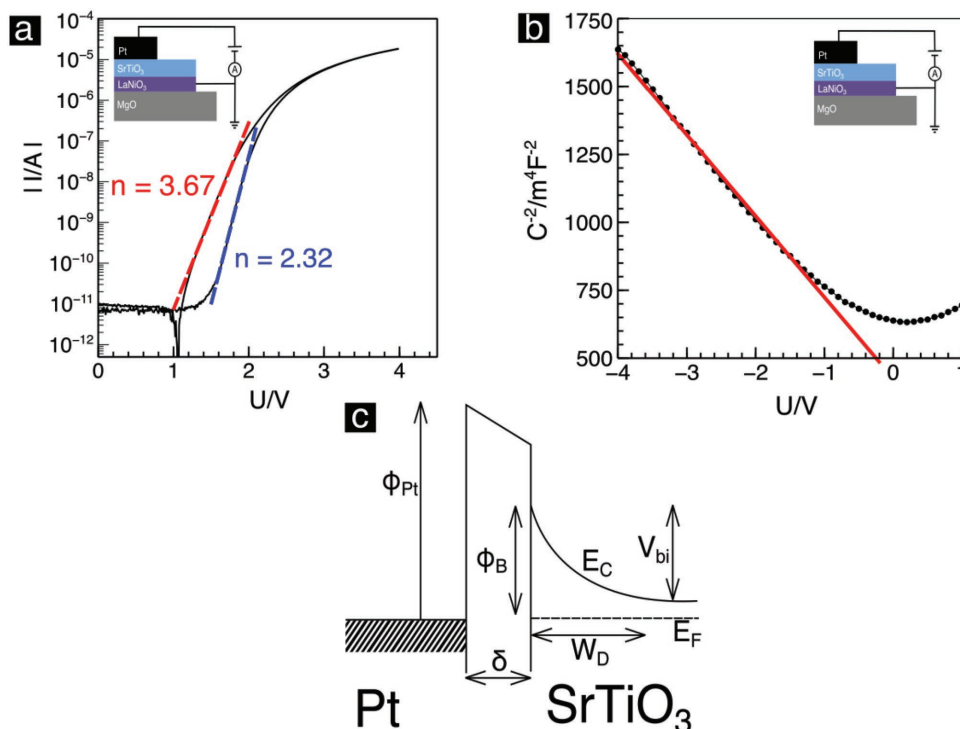


Figure 5. a) Fit to the forward bias of the LaNiO₃(bottom)/SrTiO₃/Pt(top) device using the thermionic emission model highlighting the ideality parameters of the high (blue) and low (red) resistance states. b) Capacitance–voltage measurement with the fit to the Mott–Schottky equation (Equation (4)) in red. c) Schematic of the Schottky-barrier formation at the Pt–SrTiO₃ interface where *E_C* is the conduction band edge, *V_{bi}* is the built-in voltage, *E_F* is the Fermi level, *W_D* is the depletion width, Φ_B is the Schottky barrier, Φ_{Pt} is the platinum work function, and δ is the thickness of the interfacial layer.

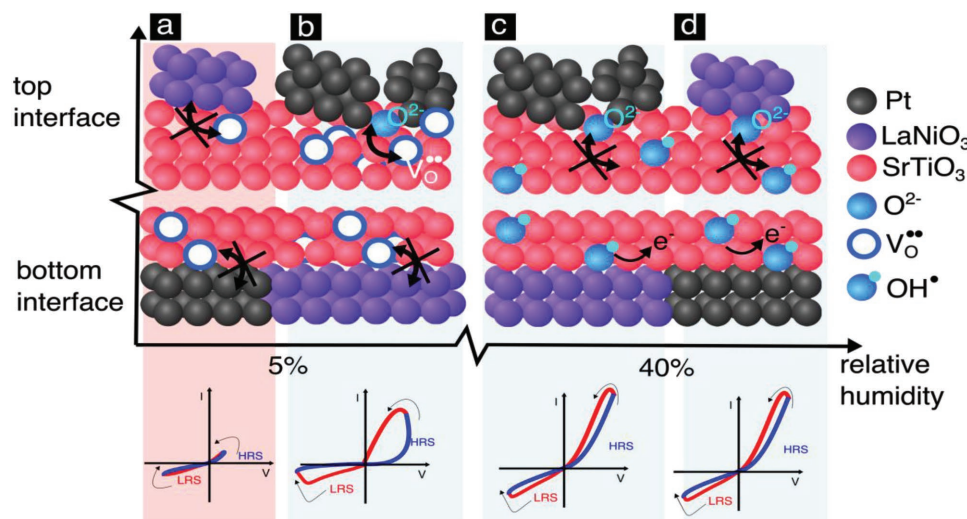


Figure 6. Schematic of the underlying mechanism for the resistive switching devices. a) The buried bottom Pt contact under dry conditions does not support oxygen ion storage and suppresses switching. b) Under dry conditions the oxygen incorporation into the nanocrystalline top Pt contact facilitates eightwise resistive switching. c, d) Under humid conditions the lesser availability of oxygen vacancies closes the hysteresis loop and impedes exchange of oxygen ions in the top contact with vacancies in the switching films.

and has not been applied to undoped SrTiO₃. According to literature, hydrogen forms a shallow donor level (Equation (2)) in many transition metal oxides^[55] including SrTiO₃,^[56,57] which can render the material an n-type conductor under humid conditions. This resulting n-type conductivity of the SrTiO₃ switching material can help to rationalize why the thermionic emission theory was applicable to describe the transport in the LaNiO₃(bottom)/SrTiO₃/Pt(top) device. Under dry conditions, the thermionic emission fit in undoped SrTiO₃ is not applicable, which can be rationalized by the higher concentration of oxygen vacancies and ionic conductivity.

2.4.2. Capacitance–Voltage Measurements

Next we turn to frequency measurements to access the capacitance voltage relationship of the interface and estimate the build-in voltage, depletion width and doping density in the device, Figure 5c. The results of the measurement at 1 kHz are shown in Figure 5b, where C^{-2} is plotted as a function of the applied bias along with a fit to the Mott–Schottky equation

$$\frac{1}{C^2} = \frac{2n^2}{qN_D\epsilon_0\epsilon_r} \left(V_{bi} - \frac{V}{n} \right) \quad (4)$$

Here C is the measured capacitance, n the ideality parameter, ϵ_0 is the vacuum permittivity, ϵ_r is the relative permittivity of SrTiO₃, N_D is the charge carrier density, and V_{bi} is the build-in voltage. The fitting parameters were the build-in voltage V_{bi} and the intrinsic doping density N_D , Figure 5c. The fitting procedure is described in more detail in the Supporting Information. From the fit we can get an approximation of the build-in voltage $V_{bi} \approx 0.64$ eV, the depletion width $W_D \approx 25$ nm and the charge carrier density $N_D \approx 10^{19}$ cm⁻³. The build-in voltage takes reasonable values, which are smaller than the extracted Schottky barrier from the thermionic-emission equation. The depletion

width is smaller than the film thickness suggesting that the film can be divided into a space charge zone and bulk. Striking here is the higher charge carrier density (N_D), especially taking into account the fact that the switching oxide is nominally undoped SrTiO₃. This supports the incorporation of hydrogen into the switching oxide, forming a shallow donor level and rendering the material n-conductive.

2.5. Switching Model

In the following we discuss the results in a switching model summarized in Figure 6, where we highlight the defect chemistry of the SrTiO₃ switching oxide under dry and humid atmospheres.

In dry atmospheres, Figure 6a,b, the lower concentration of hydroxide ions reduces the material as compared to the humid atmosphere; see also defect chemical equation (1). As a result the SrTiO₃ layer has a larger concentration of oxygen vacancies. In this case switching is completely suppressed in the Pt(bottom)/SrTiO₃/LaNiO₃(top) device; neither the bottom SrTiO₃–Pt nor the top LaNiO₃–SrTiO₃ interface facilitate switching driven by oxygen vacancies, Figure 6a. However in the LaNiO₃(bottom)/SrTiO₃/Pt(top) device, Figure 6b, the I – V hysteresis is open and eightwise switching occurs. Cooper et al. recently uncovered the mechanism for eightwise switching in dry atmospheres to be oxygen ion storage in the Pt electrode.^[19] Based on this mechanism we propose that the different microstructure of the bottom and top Pt contact, Figure S2 of the Supporting Information, is responsible for the different switching responses. The nanocrystalline top Pt contact facilitates oxygen storage and the bottom dense Pt impedes it. The top LaNiO₃ electrode also does not facilitate oxygen ion storage due to the dense microstructure and the oxygen reversibility. According to this model, we introduce an engineering strategy to suppress oxygen vacancy driven eightwise switching by burying the Schottky metal-oxide interface contact and ensuring its dense

microstructure. Since eightwise switching relies on material exchange with the atmosphere^[19] and is in competition with the filamentary counter-eightwise mechanism^[29] it would be desirable to suppress it.

Under humid conditions, Figure 6c,d, the incorporation of water significantly lowers the oxygen vacancy concentration in SrTiO₃ (Equation (1)) and proton uptake facilitates the increased n-type conductivity (Equation (2)). The resulting defect chemistry is similar to Nb:SrTiO₃ which exhibits high electronic conductivities and low oxygen vacancy concentrations.^[30] In Nb:SrTiO₃ charge trapping at the defective interface^[22] as well as reoxidation from the porous top metal contact^[23,58] have been suggested as switching mechanisms for the eightwise polarity. Reoxidation from the top contact would require the top LaNiO₃ electrode to store and supply oxygen ions, which seems improbable due to the complete switching suppression under dry atmospheres. However further studies are needed to fully understand the switching mechanism under humid atmospheres.

3. Conclusion

Recently, atmospheric humidity has been shown to play a role on Pt/SrTiO₃/Pt resistive switches,^[15] where the catalytic activity of the electrode determines the water splitting rate and subsequent oxygen incorporation.^[18] However, the role of the top electrode material on the eightwise switching mechanism in relation to atmospheric humidity and the influence of hydroxide defects in the switching remains unclear. To investigate this we have designed a model experiment where the positions of top and bottom electrode materials (Pt and LaNiO₃) were interchanged to separate the influence of the top and bottom interfaces in SrTiO₃-based resistive switches. The choice of the electrode stacking layer sequence, their catalytic activity for water splitting and their thermal history affecting the microstructure of the films and interfaces all influence the switching mechanism. In the LaNiO₃(bottom)/SrTiO₃/Pt(top) device the switching response is enhanced under dry conditions pointing to a mechanism aided by oxygen vacancies consistent with recent reports on eightwise switching SrTiO₃-based devices.^[19] However, in the Pt(bottom)/SrTiO₃/LaNiO₃(top) device switching is completely suppressed under dry conditions highlighting the necessity of ion incorporation from atmospheric humidity in the switching mechanism. Eightwise switching polarity was found in both devices despite reversing the stacking layer sequence confirming clearly that multiple switching mechanisms based on the change of defect chemistry upon humidity variation exist within the single eightwise (anomalous) switching polarity.

Summarizing, the top electrode–SrTiO₃ interface defines the location of the switching event by its relative crystalline quality and the top electrode material defines the switching response as a function of the atmospheric humidity. According to our findings it is possible to intentionally engineer electrode contacts that selectively enable resistive switching. To enable oxygen vacancy driven eightwise switching, the top electrode–oxide contact open to the atmosphere should permit

oxygen storage by its open microstructure. For suppressing the eightwise switching a buried dense metallic contact creating a high Schottky barrier at the oxide interface is desirable.

This control over the switching response has technological relevance as switching mechanisms relying on material exchange with the atmosphere might be difficult to practically implement since an atmospheric control during the device operation would be required. Our findings point out strategies to engineer electrode contacts and materials defect chemistry in order to control, and even suppress these switching mechanisms.

4. Experimental Section

Electrochemical single bits were fabricated with SrTiO₃ as the switching material and LaNiO₃ and Pt electrodes on (100) oriented single crystal MgO substrates (Crystec, Germany). The electrode top and bottom positions were exchanged in two device arrangements.

Both oxides LaNiO₃ and SrTiO₃ were grown by pulsed laser deposition (PLD, own construction) using a KrF excimer laser with a 248 nm wavelength and a substrate-target separation of 7 cm. The LaNiO₃ electrode was deposited with a laser fluence of 0.9 J cm⁻² for 5400 shots, an oxygen partial pressure of 0.03 mbar, a laser pulse frequency of 2 Hz, and a substrate temperature of 500 °C. SrTiO₃ was deposited with a laser fluence of 1 J cm⁻² for 7200 shots, an oxygen partial pressure of 0.03 mbar, a laser pulse frequency of 2 Hz, and a substrate temperature of 650 °C. The above PLD parameters will give a thickness of the LaNiO₃ layer of about 30 nm and the SrTiO₃ layer of about 60 nm. The LaNiO₃ pulsed laser deposition target was prepared via a nitrate–citrate (Pechini-type) synthesis and hot pressing. A single crystalline commercial target (Crystec, Germany) was used for the SrTiO₃ deposition.

The platinum electrodes were deposited by e-beam evaporation (Plassys MEB 550, France) with a film thickness of 80 nm. The samples were cleaned in an O₂ plasma asher (Technics Plasma TePla 100 asher system) for 60 s at 100 W before the metal evaporation.

The Pt top electrodes were defined by a standard negative resist (MicroChemicals GmbH, AZ nLof 2020) photolithography process with lift-off. The top LaNiO₃ electrodes were defined by a thick positive resist (MicroChemicals GmbH, AZ 4533) photolithography followed by Ar ion beam milling (Oxford Instruments Plasmalab 80, UK) using an argon plasma with a pressure of 30 μbar for 75 cycles of 30 s milling. The ion beam milling time was calibrated using film thickness measurements by atomic force microscopy (Asylum Research, Cypher S).

X-ray diffraction (Bruker D8 Cu Kα) patterns were acquired from experimental devices (≈200 nm thick) and are shown in Figure S1 of the Supporting Information.

HRTEM and STEM imaging (FEI, Tecnai F30 FEG S/TEM) were performed on specimens fabricated using a standard lift-out procedure in a dual-beam scanning electron microscope equipped with a focused gallium ion beam (Zeiss, NVision 40). The STEM probe size was ≈0.7 nm, and the inner and the outer collection semiangles of the annular dark field detector were 28 and 75 mrad, respectively.

Electrical DC measurements were carried out with the Keithley SMU 2601B and AC measurements with an electrochemical impedance bridge (Gamry Instruments, Reference 600TM). The sweep rate during the DC measurements was varied between 50 and 500 mV s⁻¹ and the bottom electrode was always grounded.

Supporting Information

Supporting Information is available from the Wiley Online Library or from the author.

Acknowledgements

The authors thank Dr. Morgan Trassin for his help with the pulsed laser deposition, Yanuo Shi for the TEM sample preparation by FIB, Prof. Gambardella for access to the AFM, and the staff of the FIRST clean room facilities at ETH Zurich. This work was supported by the Swiss National Science Foundation Starting Grant (Grant No. BSSGI0_155986/1). W.J.B. was a Swiss Government Excellence Scholarship holder for the academic year 2015–2016 (ESKAS No. 2015.1183) and would like to acknowledge financial support of the U.S. National Science Foundation's Graduate Research Fellowship Program (Grant No. DGE-1311230), as well as the U.S. N.S.F.'s Graduate Research Opportunities Worldwide grant.

Conflict of Interest

The authors declare no conflict of interest.

Keywords

eightwise polarity, humidity, resistive switching, strontium titanate

Received: August 24, 2018

Revised: October 2, 2018

Published online:

- [1] M. Aono, R. Waser, *Nat. Mater.* **2007**, *6*, 833.
- [2] C. J. Xue, G. Sun, Y. Zhang, J. J. Yang, Y. Chen, H. Li, *2011 Proc. 9th IEEEACMIFIP Int. Conf. Hardware Software Codesign and System Synthesis (CODESISSE)*, IEEE, Taipei, Taiwan **2011**, pp. 325–334.
- [3] J. Borghetti, G. S. Snider, P. J. Kuekes, J. J. Yang, D. R. Stewart, R. S. Williams, *Nature* **2010**, *464*, 873.
- [4] Q. Xia, W. Robinett, M. W. Cumbie, N. Banerjee, T. J. Cardinali, J. J. Yang, W. Wu, X. Li, W. M. Tong, D. B. Strukov, G. S. Snider, G. Medeiros-Ribeiro, R. S. Williams, *Nano Lett.* **2009**, *9*, 3640.
- [5] B. D. Hoskins, D. B. Strukov, F. Merrikh-Bayat, G. C. Adam, K. K. Likharev, M. Prezioso, *Nature* **2015**, *521*, 61.
- [6] G. Indiveri, B. Linares-Barranco, R. Legenstein, G. Deligeorgis, T. Prodromakis, *Nanotechnology* **2013**, *24*, 384010.
- [7] A. C. Torrezan, J. P. Strachan, G. Medeiros-Ribeiro, R. S. Williams, *Nanotechnology* **2011**, *22*, 485203.
- [8] H. Honigschmid, M. Angerbauer, S. Dietrich, M. Dimitrova, D. Gogl, C. Liaw, M. Markert, R. Symanczyk, L. Altimime, S. Bournat, G. Muller, *2006 Symp. VLSI Circuits 2006 Dig. Tech. Pap.*, IEEE, Honolulu, HI, USA **2006**, pp. 110–111.
- [9] S. Gao, F. Zeng, C. Chen, G. Tang, Y. Lin, Z. Zheng, C. Song, F. Pan, *Nanotechnology* **2013**, *24*, 335201.
- [10] V. V. Zhirnov, R. Meade, R. K. Cavin, G. Sandhu, *Nanotechnology* **2011**, *22*, 254027.
- [11] J. Maier, *Nat. Mater.* **2005**, *4*, 805.
- [12] J. J. Yang, M. D. Pickett, X. Li, D. A. A. Ohlberg, D. R. Stewart, R. S. Williams, *Nat. Nanotechnol.* **2008**, *3*, 429.
- [13] L. Michael, W. Stefan, W. Rainer, V. Ilia, *Adv. Electron. Mater.* **2017**, *4*, 1700458.
- [14] M. Lübben, P. Karakolis, V. Ioannou-Sougleridis, P. Normand, P. Dimitrakis, I. Valov, *Adv. Mater.* **2015**, *27*, 6202.
- [15] F. Messerschmitt, M. Kubicek, J. L. M. Rupp, *Adv. Funct. Mater.* **2015**, *25*, 5117.
- [16] T. Heisig, C. Baeumer, U. N. Gries, M. P. Mueller, C. L. Torre, M. Luebben, N. Raab, H. Du, S. Menzel, D. N. Mueller, C.-L. Jia, J. Mayer, R. Waser, I. Valov, R. A. D. Souza, R. Dittmann, *Adv. Mater.* **2018**, *30*, 1800957.
- [17] A. A. Haidry, A. Ebach-Stahl, B. Saruhan, *Sens. Actuators, B* **2017**, *253*, 1043.
- [18] S. Tappertzhofen, R. Waser, I. Valov, *ChemElectroChem* **2014**, *1*, 1287.
- [19] D. Cooper, C. Baeumer, N. Bernier, A. Marchewka, C. La Torre, R. E. Dunin-Borkowski, S. Menzel, R. Waser, R. Dittmann, *Adv. Mater.* **2017**, *29*, 1700212.
- [20] T. Shi, Y. Chen, X. Guo, *Prog. Mater. Sci.* **2016**, *80*, 77.
- [21] R. Merkle, J. Maier, *Angew. Chem., Int. Ed.* **2008**, *47*, 3874.
- [22] E. Mikheev, B. D. Hoskins, D. B. Strukov, S. Stemmer, *Nat. Commun.* **2014**, *5*, 3990.
- [23] C. Baeumer, N. Raab, T. Menke, C. Schmitz, R. Rosezin, P. Müller, M. Andrä, V. Feyer, R. Bruchhaus, F. Gunkel, C. M. Schneider, R. Waser, R. Dittmann, *Nanoscale* **2016**, *8*, 13967.
- [24] E. Mikheev, J. Hwang, A. P. Kajdos, A. J. Hauser, S. Stemmer, *Sci. Rep.* **2015**, *5*, 11079.
- [25] R. Muenstermann, T. Menke, R. Dittmann, R. Waser, *Adv. Mater.* **2010**, *22*, 4819.
- [26] M. Kubicek, S. Taibl, E. Navickas, H. Hutter, G. Faflek, J. Fleig, *J. Electroceram.* **2017**, *1*, 197.
- [27] F. Messerschmitt, M. Kubicek, S. Schweiger, J. L. M. Rupp, *Adv. Funct. Mater.* **2014**, *24*, 7448.
- [28] K. Szot, W. Speier, G. Bihlmayer, R. Waser, *Nat. Mater.* **2006**, *5*, 312.
- [29] M. Kubicek, R. Schmitt, F. Messerschmitt, J. L. M. Rupp, *ACS Nano* **2015**, *9*, 10737.
- [30] C. Rodenbücher, W. Speier, G. Bihlmayer, U. Breuer, R. Waser, K. Szot, *New J. Phys.* **2013**, *15*, 103017.
- [31] A. Rothschild, W. Menesklou, H. L. Tuller, E. Ivers-Tiffe, *Chem. Mater.* **2006**, *18*, 3651.
- [32] C. Lenser, A. Kuzmin, J. Purans, A. Kalinko, R. Waser, R. Dittmann, *J. Appl. Phys.* **2012**, *111*, 076101.
- [33] A. Koehl, H. Wasmund, A. Herpers, P. Guttman, S. Werner, K. Henzler, H. Du, J. Mayer, R. Waser, R. Dittmann, *APL Mater.* **2013**, *1*, 042102.
- [34] R. Dittmann, R. Muenstermann, I. Krug, D. Park, T. Menke, J. Mayer, A. Besmehn, F. Kronast, C. M. Schneider, R. Waser, *Proc. IEEE* **2012**, *100*, 1979.
- [35] A. Sawa, *Mater. Today* **2008**, *11*, 28.
- [36] G. Myburg, F. D. Auret, *J. Appl. Phys.* **1992**, *71*, 6172.
- [37] Y.-F. Chang, B. Fowler, Y.-C. Chen, F. Zhou, C.-H. Pan, T.-C. Chang, J. C. Lee, *Sci. Rep.* **2016**, *6*, 21268.
- [38] F. Zhou, Y.-F. Chang, Y.-C. Chen, X. Wu, Y. Zhang, B. Fowler, J. C. Lee, *Phys. Chem. Chem. Phys.* **2015**, *18*, 700.
- [39] T. Fujii, M. Kawasaki, A. Sawa, Y. Kawazoe, H. Akoh, Y. Tokura, *Phys. Rev. B* **2007**, *75*, 165101.
- [40] R. Schmiedl, V. Demuth, P. Lahnor, H. Godehardt, Y. Bodschnwinna, C. Harder, L. Hammer, H.-P. Strunk, M. Schulz, K. Heinz, *Appl. Phys. A: Mater. Sci. Process.* **1996**, *62*, 223.
- [41] C.-H. Chen, E. L. Hu, W. V. Schoenfeld, P. M. Petroff, *J. Vacuum Sci. Technol. B: Microelectron. Nanometer Struct.* **1998**, *16*, 3354.
- [42] J. Joshua Yang, F. Miao, M. D. Pickett, D. A. A. Ohlberg, D. R. Stewart, C. N. Lau, R. S. Williams, *Nanotechnology* **2009**, *20*, 215201.
- [43] J. D. Baniecki, R. B. Laibowitz, T. M. Shaw, C. Parks, J. Lian, H. Xu, Q. Y. Ma, *J. Appl. Phys.* **2001**, *89*, 2873.
- [44] T. Kawada, T. Ichikawa, L. Q. Han, K. Yashiro, H. Matsumoto, J. Mizusaki, *J. Electroceram.* **2004**, *13*, 715.
- [45] Z. B. Yan, J.-M. Liu, *Sci. Rep.* **2013**, *3*, 2482.
- [46] J. J. Yang, D. B. Strukov, D. R. Stewart, *Nat. Nanotechnol.* **2013**, *8*, 13.
- [47] S. Menzel, R. Waser, A. Siemon, C. L. Torre, M. Schulten, A. Ascoli, R. Tetzlaff, *2017 27th Int. Symp. Power Timing Modeling*

- Optimization and Simulation (PATMOS)*, IEEE, Thessaloniki, Greece **2017**, pp. 1–5.
- [48] S. M. Sze, K. N. Kwok, *Physics of Semiconductor Devices*, John Wiley & Sons, Inc., Weinheim, Germany **2007**.
- [49] H. Kim, C. Park, S. Lee, D.-W. Kim, *J. Phys. D: Appl. Phys.* **2009**, *42*, 055306.
- [50] E. Lee, M. Gwon, D.-W. Kim, H. Kim, *Appl. Phys. Lett.* **2011**, *98*, 132905.
- [51] M. Hansen, M. Ziegler, L. Kolberg, R. Soni, S. Dirkmann, T. Mussenbrock, H. Kohlstedt, *Sci. Rep.* **2015**, *5*, 13753.
- [52] T. Shimizu, H. Okushi, *J. Appl. Phys.* **1999**, *85*, 7244.
- [53] T. Yamamoto, S. Suzuki, K. Kawaguchi, K. Takahashi, *Jpn. J. Appl. Phys.* **1998**, *37*, 4737.
- [54] S. Suzuki, T. Yamamoto, H. Suzuki, K. Kawaguchi, K. Takahashi, Y. Yoshisato, *J. Appl. Phys.* **1997**, *81*, 6830.
- [55] A. Janotti, C. G. Van de Walle, **2007**, *6*, 44.
- [56] K. Xiong, J. Robertson, S. J. Clark, *J. Appl. Phys.* **2007**, *102*, 083710.
- [57] H. Yukawa, K. Nakatsuka, M. Morinaga, *Solid State Ionics* **1999**, *116*, 89.
- [58] R. Buzio, A. Gerbi, A. Gadaleta, L. Anghinolfi, F. Bisio, E. Bellingeri, A. S. Siri, D. Marrè, *Appl. Phys. Lett.* **2012**, *101*, 243505.